

JGR Space Physics

RESEARCH ARTICLE

10.1029/2022JA030678

Key Points:

- The diurnal and semidiurnal migrating tides are derived by multi-meteor radars in the equatorial region
- The seasonal variations of diurnal westward-propagating zonal wavenumber 1 (DW1) and semidiurnal westward-propagating zonal wavenumber 2 (SW2) observations are similar to those tidal components in Climatological Tidal Model of the Thermosphere modeling
- The unusual enhancements of DW1 and SW2 in February 2006 are possibly associated with the 2006 Northern Hemisphere stratospheric sudden warming event

Correspondence to:

X. Xue,
xuexh@ustc.edu.cn


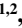











Citation:

Wang, J., Yi, W., Wu, J., Chen, T., Xue, X., Zeng, J., et al. (2022). Coordinated observations of migrating tides by multiple meteor radars in the equatorial mesosphere and lower thermosphere. *Journal of Geophysical Research: Space Physics*, 127, e2022JA030678. <https://doi.org/10.1029/2022JA030678>

Received 24 MAY 2022
Accepted 11 NOV 2022

Jianyuan Wang and Wen Yi contributed equally to this work.

Coordinated Observations of Migrating Tides by Multiple Meteor Radars in the Equatorial Mesosphere and Lower Thermosphere

Jianyuan Wang^{1,2} , Wen Yi^{1,2} , Jianfei Wu^{1,2} , Tingdi Chen^{1,2} , Xianghui Xue^{1,2,3} , Jie Zeng^{1,2} , Robert A. Vincent⁴ , Iain M. Reid^{4,5} , Paulo P. Batista⁶ , Ricardo A. Buriti⁷ , Toshitaka Tsuda⁸ , Nicholas J. Mitchell^{9,10} , and Xiankang Dou^{1,11} 

¹Deep Space Exploration Laboratory, School of Earth and Space Sciences, University of Science and Technology of China, Hefei, China, ²CAS Key Laboratory of Geospace Environment, CAS, Center for Excellence in Comparative Planetology, Anhui Mengcheng Geophysics National Observation and Research Station, University of Science and Technology of China, Hefei, China, ³Collaborative Innovation Center of Astronautical Science and Technology, Harbin, China, ⁴School of Physical Sciences, University of Adelaide, Adelaide, SA, Australia, ⁵ATRAD Pty Ltd, Thebarton, Australia, ⁶Heliophysics, Planetary Science and Aeronomy Division, National Institute for Space Research-INPE, São José dos Campos, SP, Brazil, ⁷Unidade Acadêmica de Física, Universidade Federal de Campina Grande, Campina Grande, Brazil, ⁸Research Institute for Sustainable Humanosphere (RISH), Kyoto University, Uji, Japan, ⁹Department of Electronic & Electrical Engineering, University of Bath, Bath, UK, ¹⁰British Antarctic Survey, Cambridge, UK, ¹¹School of Electronic Information, Wuhan University, Wuhan, China

Abstract We present the migrating tidal winds decomposed jointly from multiple meteor radars in four longitudinal sectors situated in the equatorial mesosphere and lower thermosphere. The radars are located in Cariri, Brazil (7.4°S, 36.5°W), Kototabang, Indonesia (0.2°S, 100.3°E), Ascension Island, United Kingdom (7.9°S, 14.4°W), and Darwin, Australia (12.3°S, 130.8°E). Harmonic analysis was used to obtain amplitudes and phases for diurnal and semidiurnal solar migrating tides between 82 and 98 km altitude during the period 2005–2008. To verify the reliability of the tidal components calculated by the four meteor radar wind measurements, we also present a similar analysis for the Whole Atmosphere Community Climate Model winds, which suggests that the migrating tides are well observed by the four different radars. The tides include the important tidal components of diurnal westward-propagating zonal wavenumber 1 and semidiurnal westward-propagating zonal wavenumber 2. In addition, the results based on observations were compared with the Climatological Tidal Model of the Thermosphere (CTMT). In general, in terms of climatic features, our results for the major components of migrating tides are qualitatively consistent with the CTMT models derived from satellite data. In addition, the tidal amplitudes are unusually stronger in January–February 2006. This result is probably because tides were enhanced by the 2006 Northern Hemisphere stratospheric sudden warming event.

1. Introduction

Dynamic processes in the mesosphere and lower thermosphere (MLT) region provide a significant key to understanding coupling processes between the lower atmosphere and the thermosphere/ionosphere system. The dynamics in the MLT region are strongly forced by atmospheric oscillations (such as gravity waves, tides, and planetary waves) originating in the lower atmosphere and are therefore dynamically coupled to the troposphere and stratosphere. In addition, the MLT region represents the lower boundary of the thermosphere/ionosphere system, and knowledge of these processes is necessary for studies of the thermosphere and/or ionosphere with regard to space weather. Among them, atmospheric tides are significant oscillations that can dominate the dynamics in the MLT region.

Atmospheric tides are global-scale atmospheric oscillations with periods that are harmonics of a solar day. These tides are predominantly generated in the troposphere and stratosphere and then propagate vertically to the MLT, where they reach large amplitudes. These atmospheric tides can be classified as migrating tides and nonmigrating tides. Migrating tides propagate westward with the apparent motion of the sun, and nonmigrating tides can propagate either westward or eastward or remain stationary. Migrating diurnal (24-hr period, westward-propagating, zonal wavenumber 1) and semidiurnal (12-hr period, westward-propagating, zonal wavenumber 2) tides are the

dominant modes that have been extensively studied. In general, 24-hr tides (diurnal tides) are dominant at low latitudes, whereas 12-hr tides (semidiurnal tides) have larger amplitudes at middle-to-high latitudes, peaking at $\sim 60^\circ$ latitude (Hagan et al., 1999).

Numerous studies have reported observations of global-scale atmospheric tides using space-based instruments because satellites can provide a global picture of the MLT wind regime (Forbes et al., 2008; Wu et al., 2006, 2008, 2011; Xu et al., 2009, 2012; Yue et al., 2013). For example, Wu et al. (2008) used the TIMED Doppler interferometer (TIDI) zonal and meridional winds to derive the global climatology of migrating and nonmigrating tides. Xu et al. (2009) reported the seasonal and interannual variations in the migrating diurnal tide in the mesosphere using temperature and wind observed by TIMED Sounding of the Atmosphere using Broadband Emission Radiometry (SABER) and TIDI measurements. Yue et al. (2013) reported the morphology of migrating terdiurnal tides with zonal wavenumber 3 using TIMED measurements. Note that these satellites, like TIMED in high inclination processing orbits, need more than 10 days (60 days) to cover 24 hr in local time, so these studies based on satellite observations can provide only the climatology of migrating tides and cannot assess the variability in global tides on short (day) time scales (Xu et al., 2009).

In addition to space-based instruments, ground-based radio radars, such as meteor radar (MR) and medium frequency (MF) radar, can provide single-point high temporal resolution and continuous MLT horizontal wind measurements at a single point (Dempsey et al., 2021; Griffith & Mitchell, 2022; Liu et al., 2022; McCormack et al., 2017; Stober et al., 2020, 2021) but have no extension in space and cannot resolve the global-scale structure. To overcome these spatiotemporal deficiencies, a few studies have combined a suitable longitudinal distribution of ground-based radars to resolve the global scale of waves such as planetary and tide waves. For example, Kleinknecht et al. (2014) presented results on quasi-stationary planetary waves 1 and 2 based on the Super DARN radar network. He et al. (2018) and He and Chau (2019) derived semidiurnal tides with different zonal wavenumbers and lunar tides by using multiple MRs, including the Juliusruh MR (12° E, 55° N), Collm MR (13° E, 51° N), Beijing MR (116° E, 40° N), Mohe MR (123° E, 54° N), and Tavistock MR (81° W, 43° N). Murphy (2003) decomposed the semidiurnal westward-propagating zonal wavenumber 1 (SW1) tidal component via MF radars situated at Davis (68.6° S, 78.0° E), Syowa (69.0° S, 39.6° E), and Rothera (67.6° S, 68.1° W) in Antarctica. Murphy et al. (2006) derived the climatology of nonmigrating semidiurnal components over the whole Antarctic continent based on 6 MF radars located in Antarctica. These studies are mainly based at high latitudes because of the rich coverage of ground-based radars. However, at low and middle latitudes, the longitudinal distribution of ground-based measurements is very scarce, which leads to an unclear understanding of global-scale tide information. On the other hand, diurnal migrating tides reach a maximum at the poles for horizontal wind due to molecular dissipation and are weaker at low latitudes (e.g., Oberheide et al., 2011; Wu et al., 2006), and some nonmigrating components, such as DE3, are important at low latitudes (e.g., Nischal et al., 2019), which poses an additional challenge to decomposing the global scale of tides from ground-based radars.

Based on the questions raised by the studies noted above, in this study, we make use of the horizontal mesospheric winds observed by four MRs near the equator, each with a similar layout and instrumentation, to which we apply the same analytical procedures and compare these results with winds from models. We analyze the parameters of the dominant migrating tides, discuss the feasibility of tidal fits by using horizontal winds from the Whole Atmosphere Community Climate Model (WACCM) data set, and compare the similarities and differences in the climatologies of these tidal components between MR observations and the Climatological Tidal Model of the Thermosphere (CTMT).

2. Data and Methods

2.1. Meteor Radar Data Set

In this study, horizontal wind data from four MRs located at Cariri (7.4° S, 36.5° W), Kototabang (0.2° S, 100.3° E), Ascension Island (7.9° S, 14.4° W), and Darwin (12.3° S, 130.8° E), hereinafter referred to as CMR, KMR, AMR, and DMR, respectively, were used. Table 1 summarizes the radar specifications, geographic coordinates, and observational time spans of the MR data set used in the current study, more detailed description of radar systems can be found in Younger et al. (2009), McIntosh (2010), Batubara et al. (2011), and Guharay et al. (2014). Figure 1 shows the geographic locations of these four MRs. The CMR is run by the National Institute for Space Research (INPE), Brazil; the DMR is run by the University of Adelaide; the AMR is run by the University of

Table 1
Geographic Locations, System Parameters, and Observational Time Periods of the MRs Used in This Study

Meteor radar	Geographic locations	Operation frequency (MHz)	Peak power (kW)	Coherent integrations	Pulse repetition frequency (Hz)	Range resolution (km)	Data used in this study
Cariri (CMR)	7.4° S, 36.5° W	35.2	12	4	2,000	2.0	1/1/2005 to 12/31/2008
Kototabang (KMR)	0.2° S, 100.3° E	37.7	12	4	2,500	2.0	1/1/2005 to 12/31/2008
Darwin (DMR)	12.3° S, 130.8° E	33.2	7.5	4	430	1.8	1/1/2005 to 12/31/2008
Ascension (AMR)	7.9° S, 14.4° W	43.5	12	4	2,144	2.0	1/1/2005 to 12/31/2008

Bath; and the KMR is a part of the CPEA project, which is supported by the Research Institute for Sustainable Humanosphere (RISH), Kyoto University.

The radar system transmitted the radio wave and coherently detected the meteor trail reflections. The range is obtained from the time interval between transmission and detection, and the azimuth and elevation angles are calculated from the phase differences between antennas. Assuming that the vertical wind is negligible, the horizontal wind can be determined by the Doppler shift following the algorithms used in Hocking et al. (2001) and Holdsworth et al. (2004).

The KMR, AMR, and DMR are used to measure horizontal winds from 80 to 100 km. Temporal and altitudinal resolutions are 1 hr and 2 km, respectively; the temporal resolution of the CMR is also 1 hr, while the altitude range of the CMR wind is available from 81 to 99 km with a resolution of 3 km. To use these data for fitting migrating tides, the vertical resolution of horizontal wind data obtained by the CMR was linearly interpolated to 2 km within the altitude range from 82 to 98 km.

As shown in Figure 2, the 24-hr oscillation is the most significant in the Lomb–Scargle (LS) periodograms (Lomb, 1976; Scargle, 1982) of the hourly zonal and meridional winds over the four stations, and the 12-hr

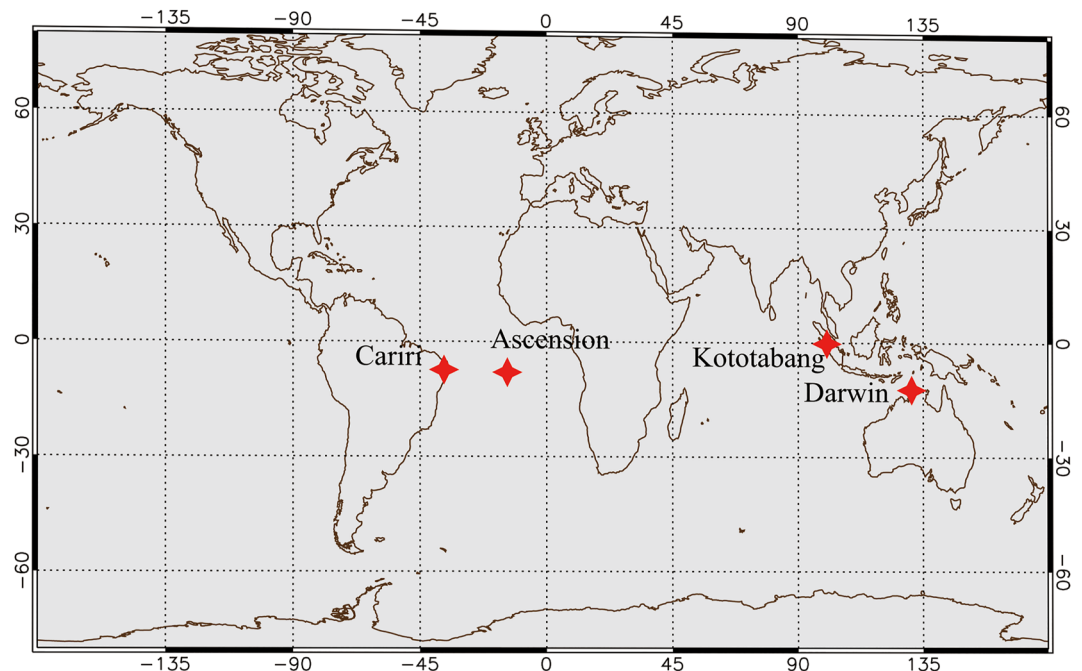


Figure 1. The locations of the four meteor radar (MR) stations used in this study.

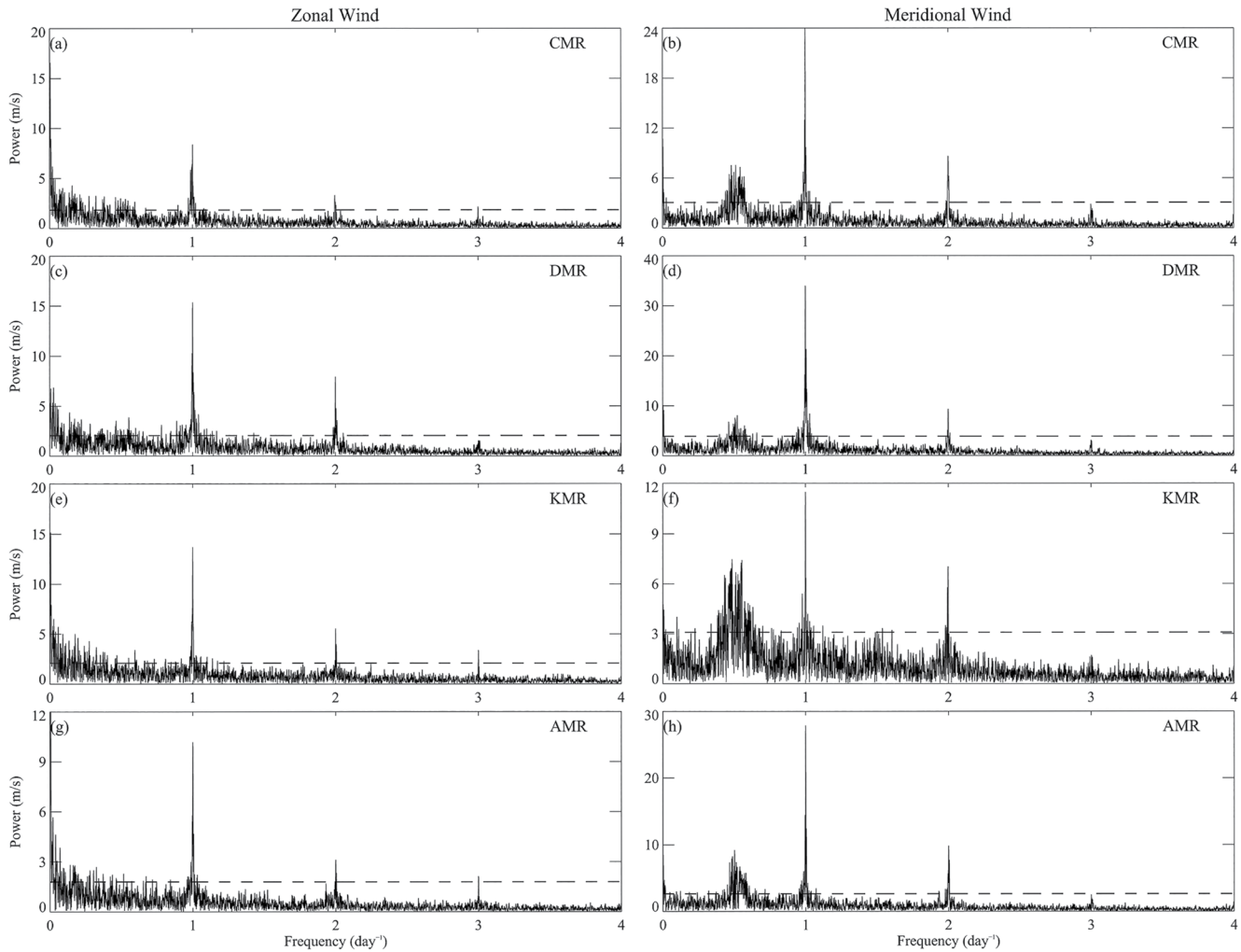


Figure 2. Lomb–Scargle analysis for the zonal and meridional winds observed by (a, b) CMR, (c, d) DMR, (e, f) KMR, and (g, h) AMR at 90 km. The black dashed lines represent the 95% significance level.

oscillation is the second-largest signal. In addition, other periods could also be found in the LS periodograms; for example, the quasi-2-day oscillation is clearly evident in the meridional wind.

Figures 3a–3h show the hourly mean zonal and meridional winds averaged during the time period from 30 January 2006 to 1 March 2006 for the four stations. Although the wind velocities differ slightly among the four stations, the wind patterns within the 82–98 km altitude range are quite similar. The dominant feature is a 24-hr diurnal oscillation in both wind components across the four MR stations. The largest anomalies of the wind velocities are approximately 80 m/s in the meridional component, and the anomalies of the zonal wind speeds are slightly weaker at approximately 50 m/s. At all stations, the downward phase propagation indicates upward wave propagation from the lower atmosphere. The phase shifts by approximately 12–16 hr within the 20 km vertical range, indicating vertical wavelengths of approximately 30–40 km.

Moreover, by comparing the meridional wind patterns in Figures 3a–3c, we note that an evident time delay of approximately 12 hr between the DMR and CMR and the longitudinal difference between the DMR and CMR is approximately 170° . Additionally, an evident time delay is approximately 10 hr between the DMR and AMR, and the longitudinal difference between the DMR and AMR is 145° . This reveals that the westward-propagating 24-hr oscillations with zonal wavenumber 1 and diurnal migrating tides are also significant in the equatorial region. In addition, the WACCM zonal winds in Figures 3q–3t not only have the most significant diurnal variations, also have a clear planetary wave 1 (PW1), while the daily mean winds observed by MRs have been removed in Figures 3a–3h and therefore not seen. To compare the PW1s between MR observations and WACCM output,

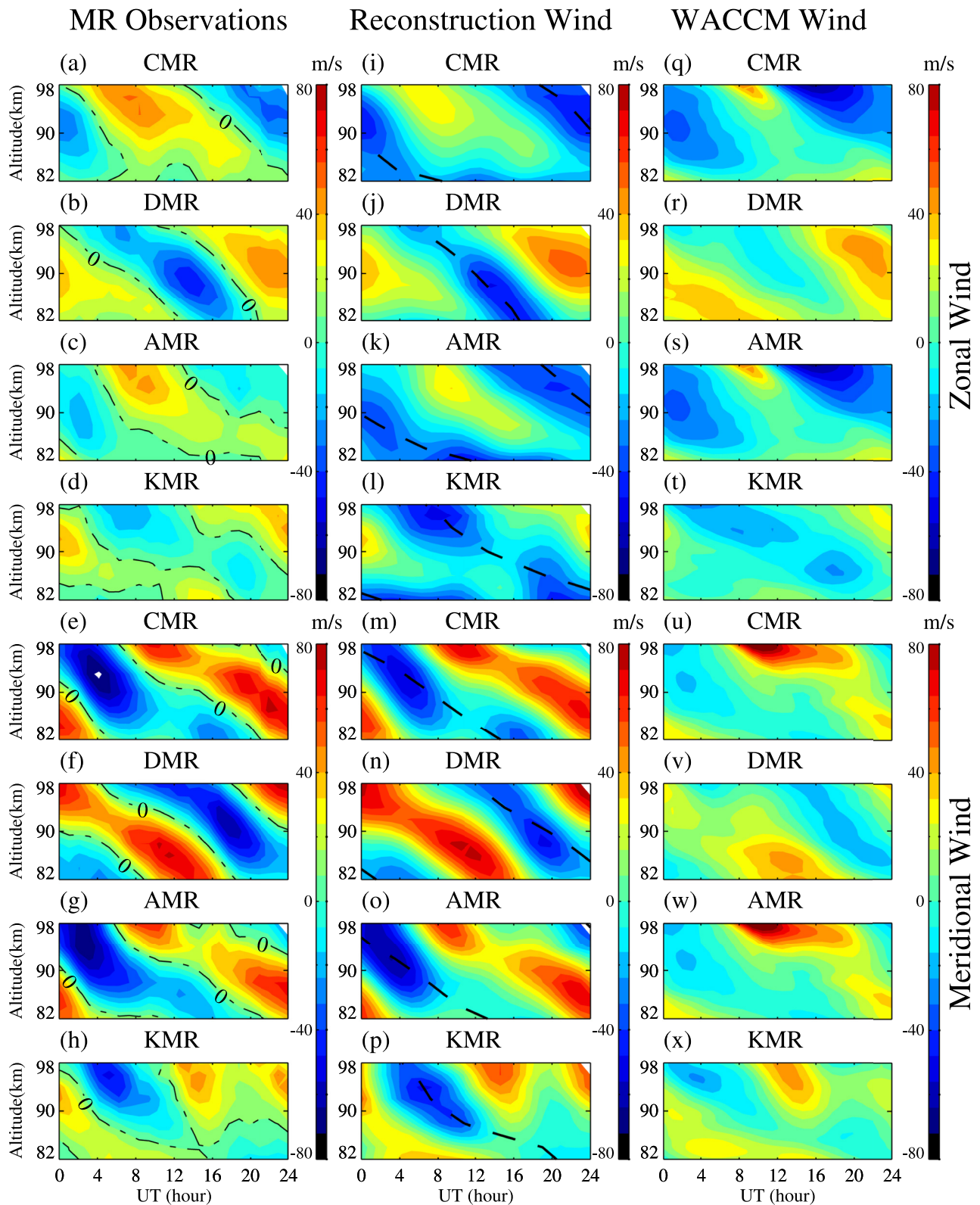


Figure 3. (a–h) Composite hourly mean zonal and meridional winds observed by the four meteor radars (MRs), CMR, DMR, AMR, and KMR, in the altitude range from 82 to 98 km averaged during the time period from 30 January 2006 to 1 March 2006. Black dotted lines in (a)–(h) indicate the zero-wind lines. (i–p) Hourly mean diurnal and semidiurnal winds reconstructed from all extracted tidal components at the four MR locations averaged during the same time period; black dashed lines in (i)–(p) indicate the minimum phase of diurnal oscillations at each altitude. (q–x) Composite Whole Atmosphere Community Climate Model (WACCM) zonal and meridional winds at the four MR locations during the same time period.

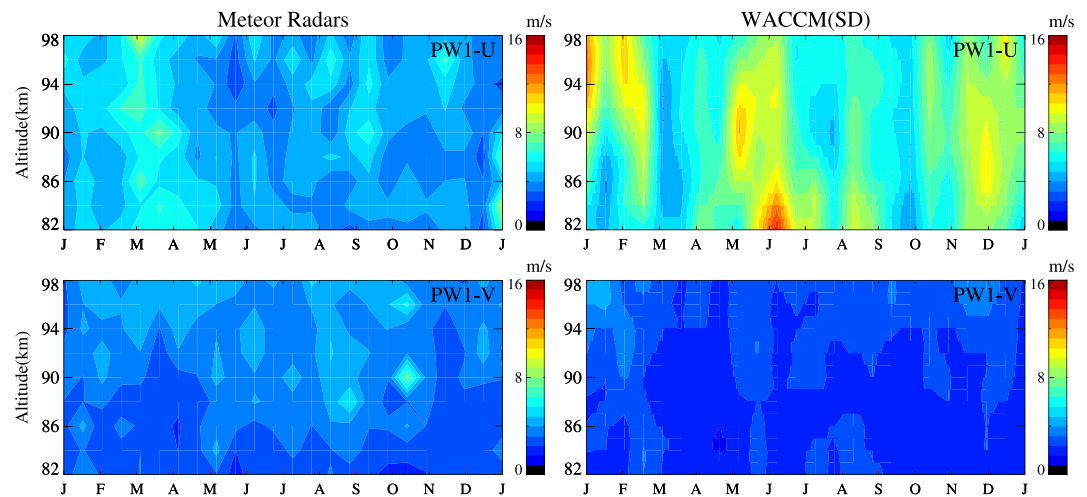


Figure 4. Meteor radar (MR) observations of the PW1 amplitudes in composite years in both wind components (in the left column) and the climatologies of the PW1 amplitudes derived from the Whole Atmosphere Community Climate Model (WACCM; specific dynamics [SD]; in the right column).

Figure 4 shows the PW1 amplitudes in both wind components derived by MR winds and WACCM (specific dynamics [SD]) output, respectively. As shown in Figure 4, the PW1s can strongly affect the zonal wind in WACCM output, but the PW1s are weaker in MR observations, which shows that WACCM has some features that are inconsistent with observations.

The diurnal and semidiurnal tides of the four radars were decomposed by least square fitting. Figure 5 presents the monthly mean amplitudes of diurnal and semidiurnal tides from 2005 to 2008 observed in the altitude range of 82–98 km at the four stations, and the observations for Cariri are also reported by Buriti et al. (2020). Also, the MR observations of wind and tides over Ascension Island have been reported by Davis et al. (2013) and Griffith et al. (2021). Figure 5 shows that both diurnal and semidiurnal tides have larger amplitudes in the meridional component than in the zonal component. For diurnal tides, the amplitudes in the meridional component are between ~5 and 65 m/s, while those in the zonal component are between ~5 and 40 m/s; for semidiurnal tides, the amplitudes in the meridional component are between ~5 and 30 m/s, and those in the zonal component are between ~5 and 18 m/s.

Figures 5a–5h show that the diurnal tidal amplitudes in both components reach their largest values in February/September and reach minima values in June. This feature is slightly different at Kototabang: the peak amplitudes occur in December–January and July–September, and the amplitudes are stronger during January–March, while the minima occur in April. In most cases, the amplitudes increase with increasing altitude, but the amplitudes at Kototabang in the meridional component in the range from 84 to 88 km are smaller than those at lower altitudes during August. At Darwin, the meridional diurnal component has large amplitudes in February and September, and these amplitudes are stronger than those at Cariri and Kototabang. This feature in February is observed in both wind components and can be captured throughout almost the entire vertical region being considered. The climatological patterns of diurnal tidal amplitudes over Ascension Island are quite similar to those over Cariri; the diurnal tidal amplitudes in zonal components over Ascension Island are slightly larger than those over Cariri.

Figures 5i–5p show that the semidiurnal tidal amplitudes in the meridional component are stronger in February, May–June, and September–November, and in particular, those amplitudes at Kototabang are smaller in October–December than at the other stations. The semidiurnal tides in the zonal component are so weak that there are no significant seasonal variations except over Darwin, showing only that the amplitudes become stronger with increasing altitude. Among the observations at KMR, the semidiurnal tides in the zonal component are largest in February–March and larger in May and December.

The diurnal and semidiurnal tidal phases at the four MRs are shown in Figure 6. In general, the diurnal and semidiurnal tidal phases are slowly variable during the year and drift with altitude for all four stations. The diurnal phase pattern for DMR in the zonal component is relatively similar to that for KMR, and both indicate that the

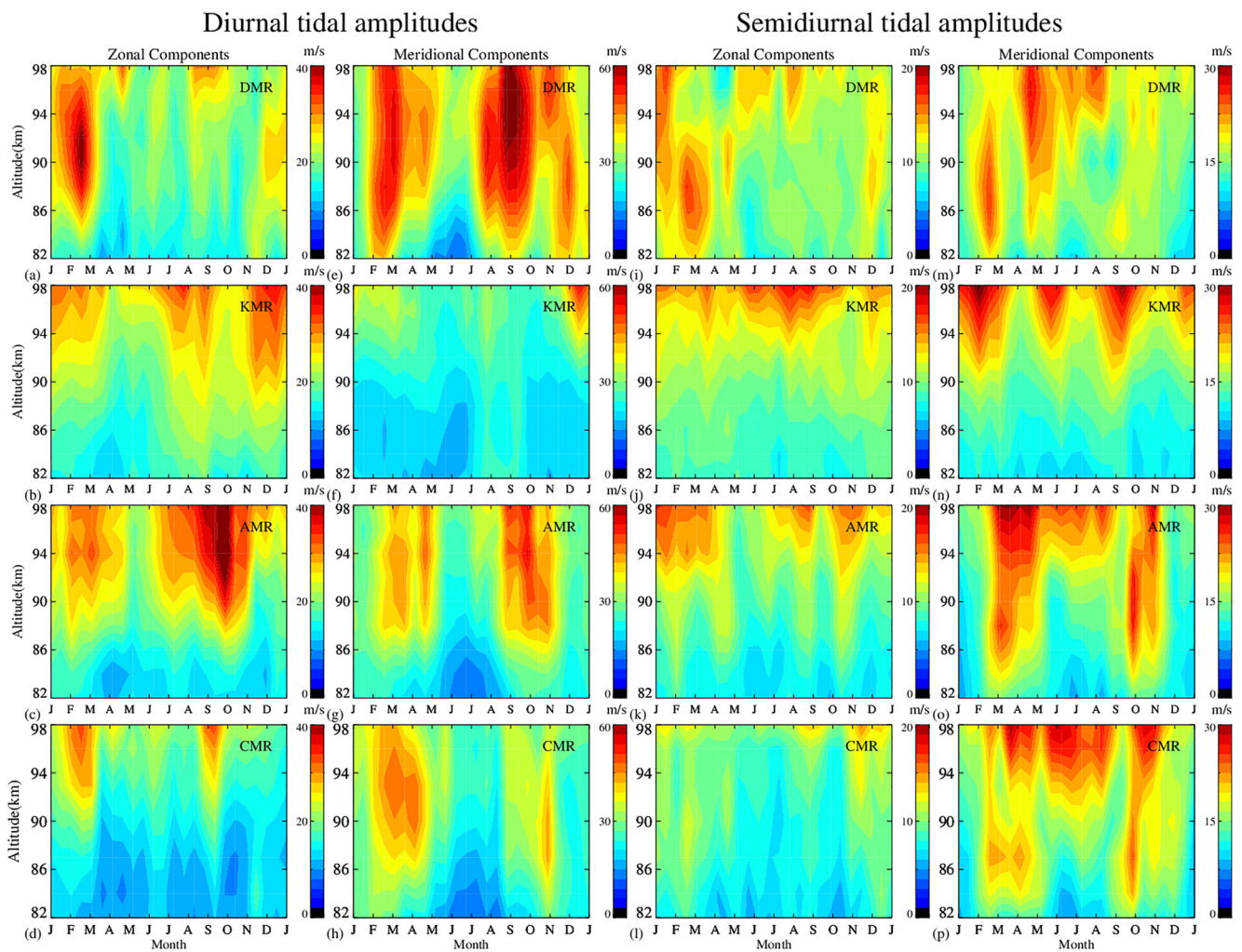


Figure 5. Climatology of (a–h) diurnal and (i–p) semidiurnal tidal amplitudes decomposed from DMR, KMR, AMR, and CMR at altitudes ranging from 82 to 98 km in zonal and meridional components. Note that the color bar values are different.

altitudes of the ~ 18 -hr phase are elevated in summer and decreasing in winter. The phase pattern for AMR is also similar to that for CMR, which may be due to the short longitudinal difference between Kototabang and Darwin as well as between Cariri and Ascension. In addition, the diurnal phase for DMR is almost opposite to that for CMR, while the semidiurnal phase for these two stations in both wind components is slightly similar. Considering that the longitudinal difference between Darwin and Cariri is $\sim 170^\circ$, these features reveal strong diurnal tides with zonal wavenumber 1 and strong semidiurnal tides with zonal wavenumber 2 in the equatorial MLT region.

By using the winds over a single MR, it is easy to calculate the diurnal and semidiurnal tides, but the migrating and nonmigrating tides cannot be separated, and the role of each tidal component cannot be clearly determined. To derive migrating tides, joint analysis of the MR winds located at four longitudinal sectors is necessary.

2.2. Decomposition Approach for Tides

In principle, the series of hourly zonal and meridional winds in the individual altitude bins from four longitudinal sectors could be used to calculate the amplitudes and phases of various tidal components, including diurnal, semidiurnal, and terdiurnal tides, with zonal wavenumbers ranging between eastward-propagating 2 and westward-propagating 2. To decrease the spatial aliasing that power from high wavenumbers leaks into lower wavenumbers, we add zonal eastward-propagating wavenumber 3 and westward-propagating wavenumber 3 to the decomposition functions.

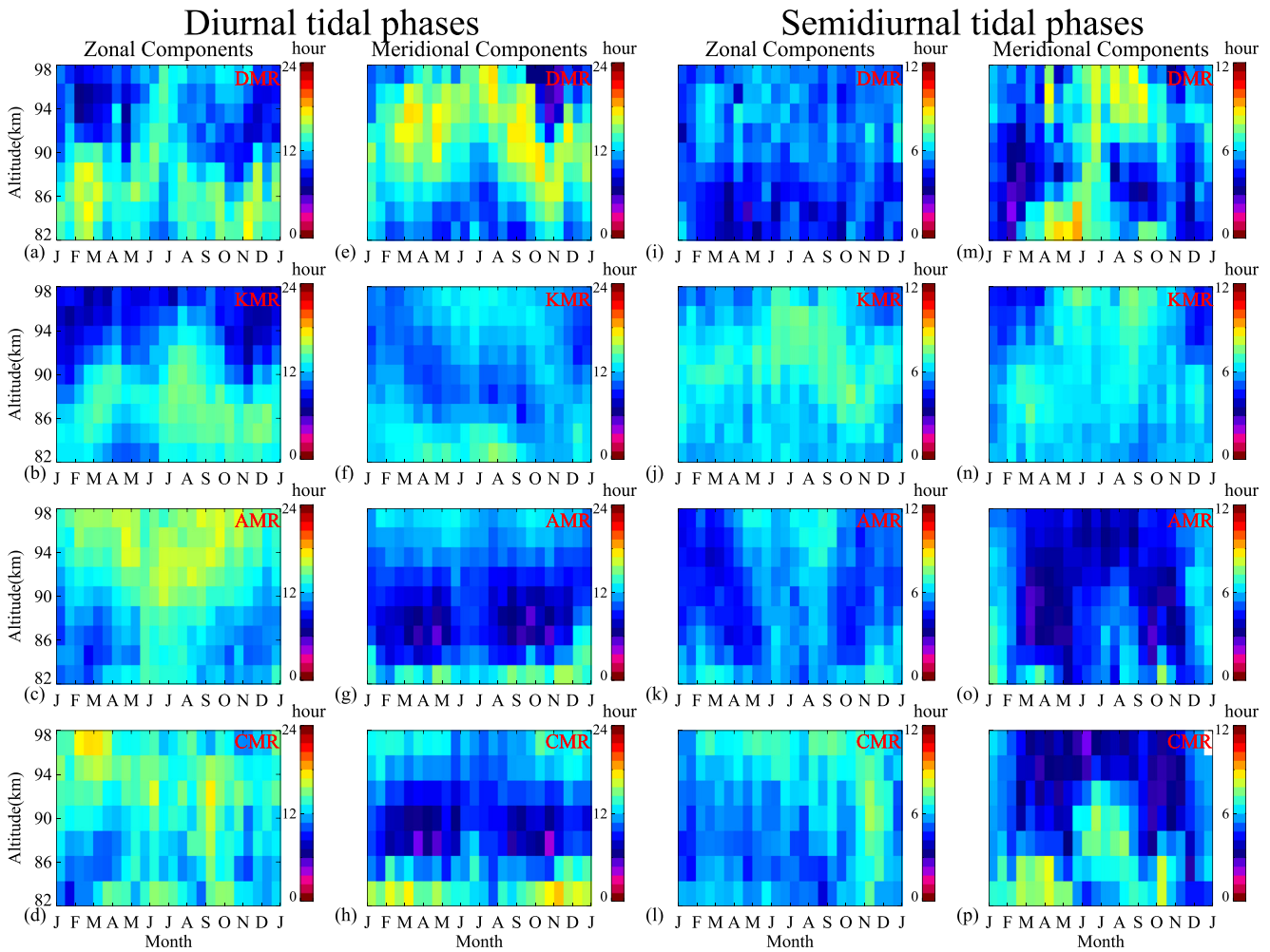


Figure 6. The same as Figure 5 but for the (a–h) diurnal and (i–p) semidiurnal tidal phases above DMR, KMR, AMR, and CMR.

A least squares fitting (e.g., Baumgarten & Stober, 2019) performed on the hourly wind data for each 3-day sliding window throughout the series could be used to decompose the tidal components DW1 and SW2, following the above function.

$$u(z, \lambda, t) = u_0(z) + \sum_{n=1}^3 \sum_{s=-3}^3 \left[a_{n,s}(z) \sin\left(\frac{2\pi n}{T}t + s\lambda\right) + b_{n,s}(z) \cos\left(\frac{2\pi n}{T}t + s\lambda\right) \right] \quad (1)$$

where u represents either the zonal or meridional wind, z represents altitude, t represents time, λ represents longitude (rad), n represents temporal wavenumber, s represents zonal wavenumber, T equals 24 hr, and u_0 represents zonal mean zonal wind.

Before using function 1, it is noted that the latitude of Kototabang is different from the other stations, which leads to the intensity of the diurnal oscillations in MLT wind over Kototabang being slightly weaker than that over the other three stations in Figures 3a–3h. Directly using function 1 to analyze the wind over four longitudinal sectors may induce additional high zonal wavenumber quantities; thus, we use the latitudinal variations obtained from the model, such as WACCM (SD), to scale the wind to make the wind over these four stations fit function 1. Furthermore, since only four MRs at different longitudinal sectors contribute to the function while there are 14 unknown coefficients related to longitude, although the hourly wind in the 72-hr window can compensate for the number of linear equations based on function 1, using a regular method to solve this linear least squares problem, such as QR or LQ factorization, is not feasible due to the singularity of the coefficient matrix. In order to obtain finite solutions, we use singular value decomposition to solve the system of linear equations. For some unusual singular values with a very small order of magnitude (e.g., less than 10^{-5}), we set the value at the corresponding

position in the inverse matrix to 0. To ensure that this processing will not produce appreciable deviations in the tidal solutions, Figures 3i–3p present the hourly mean diurnal and semidiurnal winds reconstructed from all extracted tidal components. The reconstructed winds are quite similar to each of the four MR observations, which indicates that our decomposition method is feasible at least in terms of calculation.

2.3. Credibility of the Method Used to Derive Tides

Due to the sparsity of the longitudinal distribution, an analysis of the topological aspect of the extraction method, function 1, is necessary. For the tidal component with zonal wavenumber 1, these four MRs can cover $\sim 180^\circ$ longitudinal phase variations; for that with zonal wavenumber 2, these radars can cover $\sim 90^\circ$ longitudinal phase variations for two zonal wavelengths. Covering half of the longitudinal phases is solvable but may affect the credibility of the solution. To further discuss the influence of station longitudinal distribution on the fitting method, it is necessary to use a high-resolution MLT wind model; WACCM is a model that has high temporal and spatial resolution and satisfactory credibility for neutral winds in the MLT region and could be used to simulate MLT tides (Pedatella et al., 2012; Smith et al., 2017; Yang et al., 2018).

WACCM is a high-top model based on the Community Earth System Model (version 1) framework (Hurrell et al., 2006), which is an optional variation of the Community Atmosphere Model version 4 (CAM4) that has been designed to investigate the interactions among chemistry, radiation, and dynamics and their impact on the Earth's climate system (Neale et al., 2013). The current study uses the SD version of WACCM, in which neutral temperatures and winds below 50 km are nudged toward NASA's Modern-Era Retrospective analysis for Research and Applications (MERRA; Lamarque et al., 2012). The present integrations have a horizontal resolution of 2.5° in longitude and 1.9° in latitude. There are 144 vertical levels, and the vertical resolution is approximately 0.5 km, ranging from 80 to 100 km. The time step is 30 min.

Figures 3q–3x present the WACCM (SD) winds in the MLT region averaged during the time period from 2005 to 2008 at the locations of the four MR stations. Comparison of these winds with the winds observed from MRs reveals that the wind patterns are very similar, although the oscillations in the meridional components of the WACCM winds are slightly weaker than those in the MR observations. In the past, WACCMs were compared to other MLT wind data sets, such as MR observations, and discussed agreements and deviations of the seasonal variations in mean winds and tides (e.g., Pancheva et al., 2020; Stober et al., 2021; Zhou et al., 2022). Usually, the MR-observed tidal amplitudes are slightly larger than those in the WACCM output. The tidal correspondence between observations and model output in the MLT region strongly depends on the forcing in the troposphere and tropopause for migrating tides (Ortland, 2017). Thus, the difference between the MR-observed tidal amplitudes and that in the WACCM output may be related to the tropospheric/stratospheric water vapor and ozone in the reanalysis data used for WACCM (SD), which determine the radiative forcing. Additionally, general circulation models often depend on gravity wave parameterizations, while gravity waves interact with tides (Ortland & Alexander, 2006; Watanabe & Miyahara, 2009), which could also cause the difference. Although the tides in the WACCM output are slightly different from the observations, the WACCM could still be used to discuss the fit method from a topological perspective considering that the diurnal wind patterns of the WACCM output and MR observations are similar.

To discuss the method for decomposing tides via four longitudinal sectors, a method for extracting tides via full longitudes is proposed below. Least squares fits are performed on the wind data for each 3-day sliding window throughout the series, and only days with data that are available for more than 18 hr each day are used. Because the WACCM zonal and meridional wind data are available on a global scale, the zonal wavenumber is taken from eastward-propagating 7 to westward-propagating 7 for fitting all tidal components. In addition, it should be noted that quasi-2-day oscillations may also contribute to neutral winds in the 3-day window, so these quasi-2-day components with all zonal wavenumbers should be added to the tidal fits.

Following the above method, the meridional or zonal wind variations in time and longitude at a given altitude can be written as follows:

$$u(z, \lambda, t) = u_0(z) + \sum_{n=1}^3 \sum_{s=-7}^7 c_{n,s}(z) \cos\left(\frac{2\pi n}{T}t + \frac{2\pi s}{2\pi}\lambda + \varphi_{n,s}(z)\right) + \sum_{s=-7}^7 c_{4,s}(z) \cos\left(\frac{2\pi}{2T}t + \frac{2\pi s}{2\pi}\lambda + \varphi_{4,s}(z)\right) \quad (2)$$

Tidal amplitudes at 86 km based on WACCM dataset

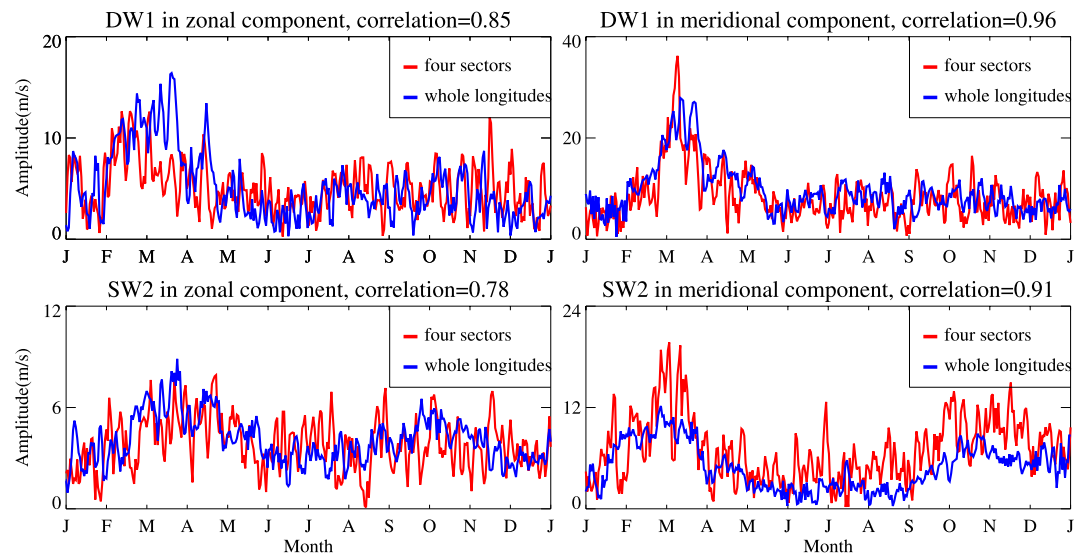


Figure 7. Correlation coefficients between the four-point fitting and whole longitude fitting for DW1 and SW2 tidal amplitudes in both wind components at 86 km obtained from Whole Atmosphere Community Climate Model (WACCM) winds in composite years.

where u represents either the zonal or meridional wind; z represents altitude; t represents time; λ represents longitude (rad); n represents temporal wavenumber; s represents zonal wavenumber; T equals 24 hr; φ represents phase; u_0 represents zonal mean zonal wind; the second section represents tidal components comprising 24-, 12-, and 8-hr oscillations; and the third section represents quasi-2-day oscillation components.

The MLT winds of the WACCM are used to extract tides at altitudes ranging from 82 to 98 km at 5°S with whole longitudes by using function 2; then, the horizontal winds at the four locations of Cariri, Kototabang, Ascension, and Darwin are used to decompose the tidal components of DW1 and SW2 by function 1. Figure 7 compares the tidal amplitudes at 86 km derived by the whole longitudes with the four-point fitting results and calculates the correlation between the two results for each tidal component. For both migrating components, the seasonal features of the full longitude fitting and the four-point fitting are very similar, and their correlations are satisfactory; all correlations are higher than 0.85 except that in SW2-U, 0.78. For the meridional components, the correlation coefficients are already higher than 0.9. These results have shown that the four-point fitting amplitudes of DW1 and SW2 are quite close to the whole longitude fitting. In the tidal fitting based on the WACCM, the four-point fitting tidal amplitudes are satisfactory in fitting the migrating tides with zonal wavenumbers 1 and 2.

3. Migrating Tidal Components Observed by the Four Meteor Radars

To derive the migrating tides, the four MRs were jointly analyzed by function 1 to calculate amplitudes and phases for all dominant tidal components.

The left column in Figure 8 shows the monthly mean amplitudes of diurnal and semidiurnal migrating tides in composite years at altitudes ranging from 82 to 98 km. The diurnal migrating tides have amplitudes between ~1 and 15 m/s in both components, and the semidiurnal tidal amplitudes reach the same maximum of 12 m/s in the zonal component, while the maxima of these amplitudes in the meridional component are stronger at approximately 15 m/s. The diurnal migrating tides in both components exhibit almost the same pattern, with amplitude maxima in March and September and minima in June. For the semidiurnal migrating tides, the amplitudes peaked in February–March and in the region above 94 km in June, showing similar seasonal variations in migrating tidal amplitudes in both components.

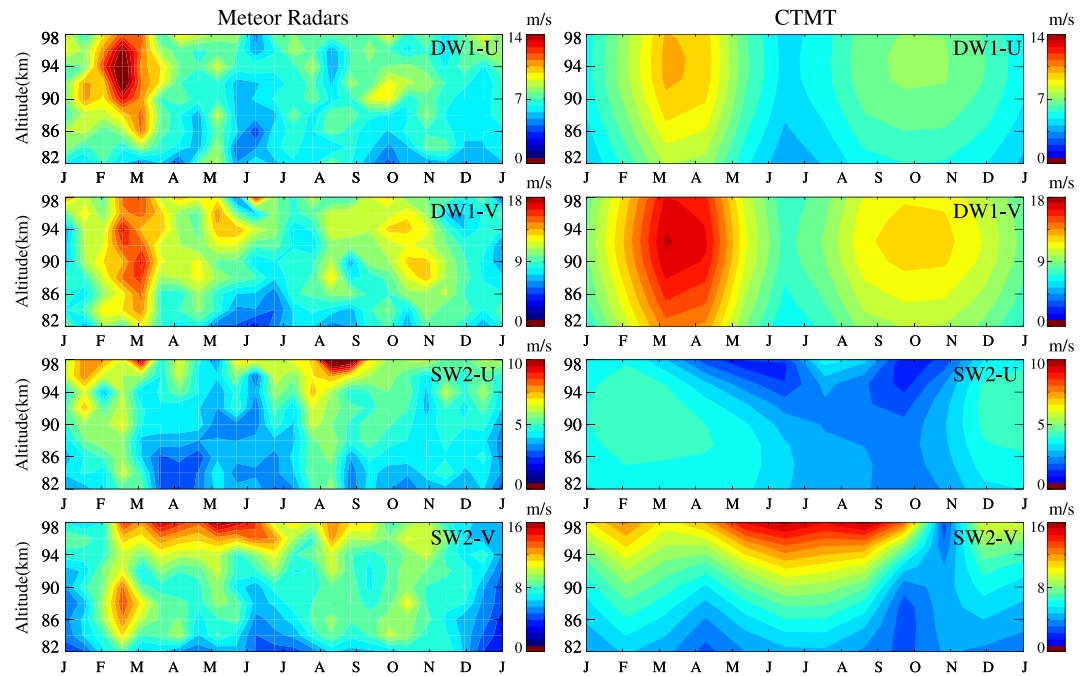


Figure 8. Meteor radar (MR) observations of the DW1 and SW2 tidal amplitudes in composite years in both wind components (in the left column) and the climatologies of the DW1 and SW2 tidal amplitudes derived from the Climatological Tidal Model of the Thermosphere (CTMT; in the right column). Different scales for the color bars show the different maxima of amplitudes for these tidal components.

If directly using function 1 to derive the migrating tidal phases, it will lead to a high time variability in the phases; a frequency shift methodology (Stober et al., 2020) could be used to correct the phase. As shown in Figure 9, tidal component phases (Universal Time of maxima at the longitude of 0° in hours) are observed earlier in the zonal component than in the meridional component at most altitudes, and these phases are approximately symmetrical around July at all altitudes considered. The phase differences between the zonal and meridional components, shown in Figures 9e and 9f, are mostly equal to -6 and -3 hr (equivalent to -90°) for the diurnal and semidiurnal tides, which are consistent with previous results (Liu et al., 2020; Oberheide et al., 2006). In addition, the vertical phase differences of DW1 migrating tides are approximately 12–15 hr, meaning that the

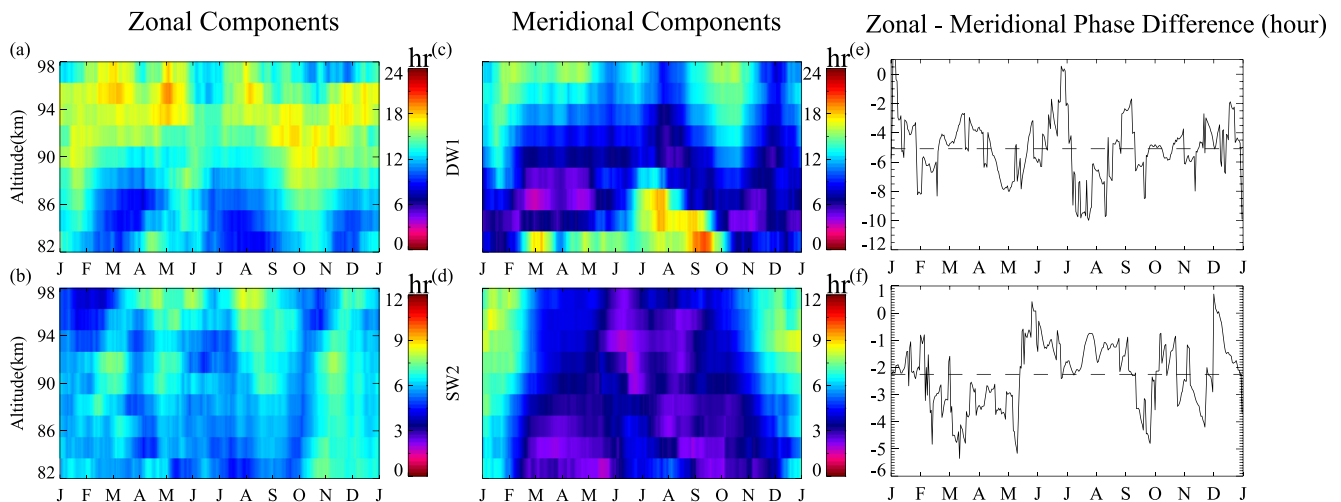


Figure 9. (a, b) Monthly mean tidal phases in composite years for the DW1 and SW2 tidal components in zonal components at altitudes ranging from 82 to 98 km derived from the four meteor radars. (c, d) Same as (a) and (b) but in meridional components. (e, f) Phase differences between zonal and meridional components averaged over the altitude range of 82–98 km for DW1 and SW2; the dotted lines indicate the average phase differences.

vertical wavelength of DW1 migrating tides is 30–40 km (qualitative estimation) and that in the zonal component are slightly larger than in the meridional component; the vertical phase differences of SW2 tides are approximately 4 hr in the zonal component and 6 hr in the meridional component, meaning that the vertical wavelengths of SW2 tides are ~60 and ~40 km, respectively. However, this vertical wavelength for DW1 tides derived by MR observations is slightly larger than that derived from TIDI observations (~20 km) in Wu et al. (2006). In past observations, different instruments obtained different vertical wavelengths. For example, She et al. (2016) analyzed lidar temperature observations in the mesopause region and deduced that the vertical wavelength of temperature diurnal tides is ~40 km in January. López-González et al. (2017) calculated that the vertical wavelength of semidiurnal tides is ~35 km derived from O₂ atmospheric and OH(6-2) airglow SATI observations. Also, the results in the model output are a bit different. Chang et al. (2008) suggested that the vertical wavelengths for DW1 tides in the WACCM output are 25–30 km in the low to midlatitude MLT region, while that in the GSWM is ~28 km. Note that the vertical wavelengths decomposed from the four MR observations are larger than those in the model, while those derived by the TIDI are shorter than the model output. The TIDI tides are based on 60-day running mean wind TIDI data and thus are not sensitive to short-term variation, but the fit method to decompose tides from multiple MRs is based on 3-day running mean data, and sensitivity to short-term variations may lead to a greater difference in tidal phase, which in turn affects the vertical wavelength. On the other hand, the nonmigrating tides are significant at low latitudes (Nischal et al., 2019), such as DE3, and the vertical wavelength for that nonmigrating component is larger than that for DW1. Due to the sparsity of the longitudinal distribution of MRs, some power from the high zonal wavenumber nonmigrating component may unavoidably leak into the DW1 component, which could lead to a large vertical wavelength.

For further discussion, we compared the observation results with the CTMT. The CTMT is derived from TIDI, SABER, and Challenging Minisatellite Payload (CHAMP), as proposed and completed by Oberheide et al. (2011), and the validation of this model in the MLT region was provided in their work. This software is a three-dimensional (time, altitude, and latitude) model that is based on tidal observations made in the MLT region that are extended into the thermosphere using Hough mode extension (HME) modeling as a function of latitude (from 90° S to 90° N), altitude (from 80 to 400 km), and month (from January to December). The observation data comprise the TIDI zonal and meridional wind tides, SABER temperature tides, and CHAMP neutral density tides in the 2002–2008 composite years. The CTMT provides the 14 most significant diurnal and semidiurnal tidal components for temperature, density, and zonal, meridional, and vertical winds, including DW2, DW1, D0, DE1, DE2, DE3, SW4, SW3, SW2, SW1, S0, SE1, SE2, and SE3. In addition, CTMT is valid only for 110 solar flux units (sfu) due to the tidal dissipation sensitivity to thermospheric temperature. Figure 8 presents the DW1 and SW2 tidal amplitudes in both wind components in the altitude range from 82 to 98 km obtained from the CTMT modeling and MR observations. In the right column, the CTMT results show that the diurnal migrating tides, DW1, reach the largest value in March and have the second strongest amplitudes in October in both wind components. Notably, the DW1 tidal amplitudes in the meridional components are larger than those in the zonal components, and other MR observations at low latitudes also support this point, such as the observations by the Kunming MR (Yi et al., 2019; Zhao et al., 2012) and the Fuke MR (Jiang et al., 2010). These climatological features are similar to our fitting results by the four MRs in the left column, and the maximum observed DW1 amplitude in zonal component is 12 m/s, which is larger than the CTMT output of 9 m/s. The observed semidiurnal migrating tides, SW2, in the zonal components are also larger, approximately 8 m/s, than the 5 m/s CTMT results. Note that the maximum of migrating tidal amplitudes observed by MRs in zonal component are ~3 m/s larger than those in CTMT output. Considering that the CTMT does not capture the migrating tides forced in situ (Oberheide et al., 2011), thus, the slight differences between observations and modeling are acceptable. The SW2 amplitudes in the meridional components are stronger from December to October of the next year; SW2 amplitudes in the zonal components are larger from December to May of the next year and peak in July over 95 km. Compared with the CTMT results, the SW2 amplitudes based on MRs in the zonal components are stronger from December to April of the next year and peak from June to August over 95 km, which may be due to the lack of radar data in April and July–August. The observed SW2 amplitudes in the meridional components are larger from February to September, but the altitude of the maximum in February is approximately 10 km lower than the CTMT results, and the weaker amplitudes in October–November are not shown. Considering that the SW2 tides in CTMT are derived around the HME methodology and SABER observations and due to the orbital geometry between the ascending and descending branches, the semidiurnal tides may not be well constrained.

Tidal Amplitudes Residual During 2006 SSW

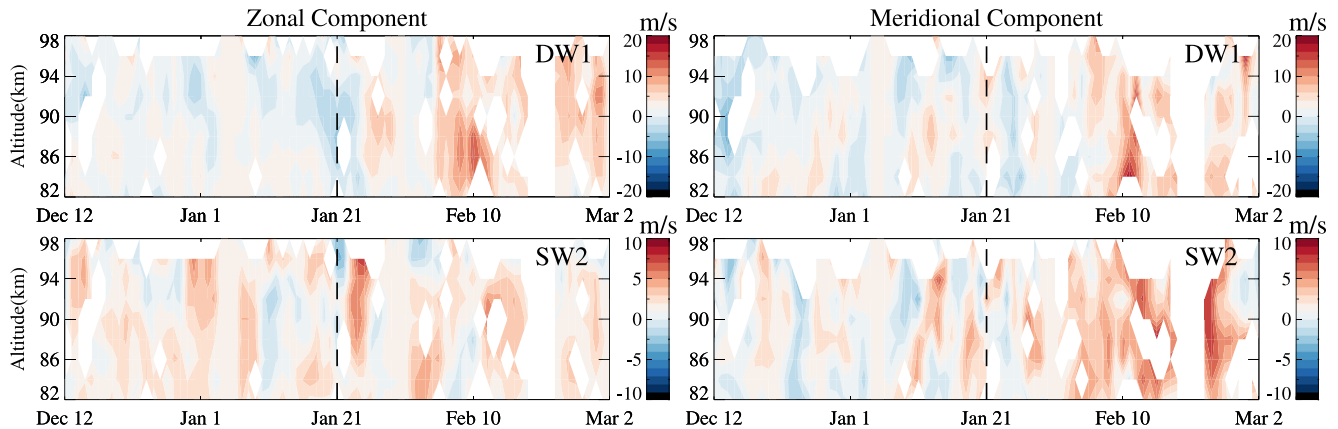


Figure 10. The DW1 and SW2 tidal amplitude residuals during the time period from 12 December 2005 to 2 March 2006 for both wind components at altitudes ranging from 82 to 98 km. The dotted lines indicate 21 January 2006. Different scales for the color bars show the different maxima of amplitudes for these tidal components.

4. Response of Migrating Tides to the 2006 Stratospheric Sudden Warming Event

In addition, the DW1 and SW2 tidal components in both zonal and meridional components from MRs reach unusual peak amplitudes in February 2006 (not shown here). A series of studies have reported that the major stratospheric sudden warming (SSW) in 2006 could have had an effect on tidal propagation in the MLT region (Hoffmann et al., 2007; Paulino et al., 2011; Sridharan et al., 2009). SSW events are a major phenomenon in the winter polar region. The significant feature of these events is that over the course of a few days, the westerly stratospheric polar vortex in the winter hemisphere is disrupted, and the midstratospheric temperatures increase rapidly by up to 40 K (Andrews et al., 1987). A major SSW event occurs when the stratospheric temperatures increase and the zonal mean circulation at 60° latitude at 10 hPa reverses; an SSW could be classified as a minor event when the temperatures increase, but the zonal mean circulation at a pressure level of 10 hPa does not reverse (McInturff, 1978). In the research of Butler et al. (2015), the 2006 Northern Hemisphere SSW (NH-SSW) was classified as a major SSW event. Although SSW events mainly occur in the polar stratosphere, they can also strongly affect vertical coupling over a large range of altitudes from the ground surface up to the MLT/ionosphere (e.g., Chau et al., 2012; L. Goncharenko & Zhang, 2008; L. P. Goncharenko et al., 2013; Li et al., 2021; Matsuno, 1971; Pedatella & Forbes, 2010; Ye et al., 2021). Figure 10 presents the DW1 and SW2 tidal amplitude residuals, which are these tidal amplitudes minus the seasonal variations in these tidal components, and the dotted lines indicate the SSW central day, that is, 21 January 2006. In the zonal components, DW1 amplitudes exhibit major enhancement after 21 January, and the amplitudes peak on approximately 15 February. The SW2 amplitudes are also weakly enhanced on 26 January. In the meridional components, the DW1 and SW2 amplitudes both exhibit enhancement after the 2006 SSW central day, and the amplitudes also reach a maximum on approximately 15 February.

To prove that the 2006 NH-SSW event was related to the enhancement of migrating tides after 21 January 2006, Figure 11 shows the residuals of diurnal and semidiurnal tidal amplitudes based on the Kototabang MR, representing the difference between the tidal amplitudes during the 2006 SSW event and the amplitudes on the corresponding date in the composite year. A Monte Carlo test was used to evaluate the statistical significance of the residual for the SSW. In this analysis, the time series that follows the uniform distribution was generated randomly. By performing the Monte Carlo procedure 4,000 times, the residual during the 2006 NH-SSW event was compared with the values from the 4,000 calculations to determine the statistical significance. The areas covered with circle symbols denote 90% significance according to the Monte Carlo test, and the areas covered with cross symbols denote 95% significance according to the same test. In the zonal components, the enhancement of diurnal and semidiurnal tides is weaker; the diurnal tidal amplitudes increase mainly on 10 February, and the semidiurnal tides are enhanced from 21 January to 2 February. In the meridional components,

Tidal Amplitude Residuals Over Kototabang During 2006 SSW

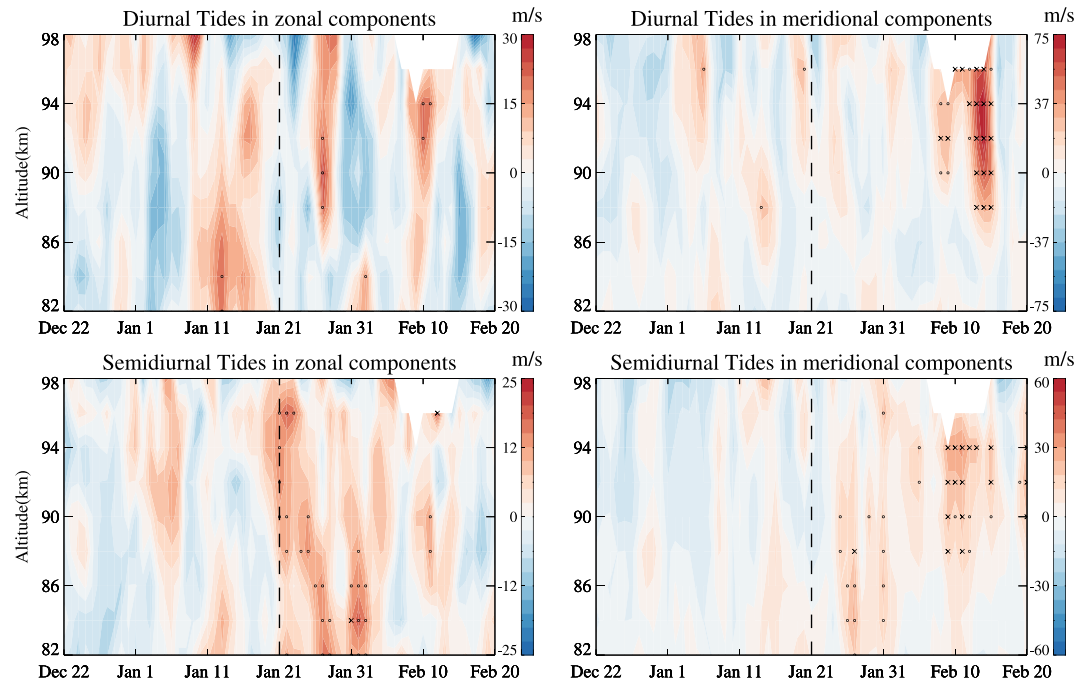


Figure 11. Diurnal and semidiurnal tidal amplitude residuals in both wind components over Kototabang during the time period from 22 December 2005 to 20 February 2006. The stippled areas indicate 90% significance according to the Monte Carlo test, and the areas covered with cross symbols denote 95% significance according to the same test. The black dashed lines indicate 21 January 2006. Different scales for the color bars show the different maxima and minima of residuals for these tidal components.

the enhancement of both diurnal and semidiurnal tides is very significant; the diurnal and semidiurnal tides are both enhanced from 10 February to 15 February by the 2006 NH-SSW event at over 95% significance. There is a 20- to 25-day delay in the response of the tides to the SSW event, which was reported by Lima et al. (2012). Besides, Eswaraiah et al. (2017) also reported that semidiurnal tides in Antarctica responded to a Southern Hemisphere SSW (SH-SSW) after a 35-day delay. Based on the results of Figure 10, in the zonal components, the minor enhancement of the SW2 amplitudes may be related to the SSW event, but the causal relationship between the DW1 amplitudes and the SSW event is unclear. According to the enhancement times on 26 January and 10 February, the DW1 tide response to the SSW event may exist. In the meridional components, the SW2 amplitudes are clearly modulated by the SSW event. Since the DW1 tides are the most dominant components near the Kototabang latitude, the major enhancement of the diurnal tides in the meridional components over Kototabang should mainly be contributed by the DW1 tidal component, which means that the enhancement of the DW1 tides in the meridional component in Figure 11 is the result of SSW event modulation.

5. Summary

Horizontal winds observed by the four MRs in the equatorial MLT region are used to derive migrating tides. The neutral wind data were from 1 January 2005 to 31 December 2008 and derived from the MRs at Cariri (7.4°S, 36.5°W), Kototabang (0.2°S, 100.3°E), Ascension Island (7.9°S, 14.4°W), and Darwin (12.3°S, 130.8°E). According to the tidal fitting simulation based on WACCM winds, the migrating tides could be extracted accurately by the four MRs.

The migrating tidal amplitudes obtained from these four MRs exhibit significant seasonal and altitudinal variations, and their phases are slightly different between the two wind components. For all tidal components, the monthly mean amplitudes in the meridional components are larger than those in the zonal components. The largest diurnal migrating tidal amplitudes are approximately 17 m/s, which also occur in the meridional component.

The diurnal migrating tidal amplitudes are strongest in March, reach their second-largest amplitudes in October, and are weakest in June in both wind components. The semidiurnal migrating tidal amplitudes are stronger from February to October and weaker from September to November. These features are very similar to the results from the CTMT. Nearly, all tidal amplitudes are unusually stronger in February 2006 in both wind components, which may be the response of tides to 2006 NH-SSW modulation, causing enhancement in February.

In this study, we report a method to decompose migrating tidal winds by jointly analyzing four MRs over the equatorial MLT region. The results presented in this study will provide an observational basis for further modeling studies of migrating tidal dynamics impacts on the MLT region. In addition, our results will also provide a chance to investigate the coupling between the lower and middle atmosphere through the Madden and Julian Oscillation (Eckermann & Vincent, 1994; Madden & Julian, 1994) modulated by upward-propagating tides. A study of the interseasonal periodicity of migrating tidal winds will be reported in a subsequent paper.

Data Availability Statement

The Kototabang meteor radar data are available from http://database.rish.kyoto-u.ac.jp/arch/iugonet/mwr_ktb/index_mwr_ktb.html. The Ascension Island meteor radar data are available from <https://data.ceda.ac.uk/badc/meteor-radars/data/ascension>. The Cariri meteor radar data are available from <https://doi.org/10.5281/zenodo.6575792>. The Darwin meteor radar data are available from <https://doi.org/10.5281/zenodo.6575832>. The SD-WACCM data set utilized in the current study is available at <https://doi.org/10.12176/01.60.00003-V01>. The CTMT data sets are available from <https://doi.org/10.5281/zenodo.5541913>.

References

- Andrews, D. G., Holton, J. R., & Leovy, C. B. (1987). *Middle atmosphere dynamics* (p. 489). Academic Press. <https://doi.org/10.1002/qj.49711548612>
- Batubara, M., Suryana, T., Manik, T., & Sitompul, P. (2011). Kototabang–West Sumatera meteor radar: System design and initial results of a large scale meteor echo. *Paper presented at the 6th International Conference on Telecommunication Systems, Services, and Applications, Bali Denpasar, Indonesia* (pp. 17–21). <https://doi.org/10.1109/TSSA.2011.6095399>
- Baumgarten, K., & Stober, G. (2019). On the evaluation of the phase relation between temperature and wind tides based on ground-based measurements and reanalysis data in the middle atmosphere. *Annales Geophysicae*, 37(4), 581–602. <https://doi.org/10.5194/angeo-37-581-2019>
- Buriti, R. A., Hocking, W., Batista, P. P., Paulino, I., Paulino, A. R., Garbanzo-Salas, M., et al. (2020). Diurnal mesospheric tidal winds observed simultaneously by meteor radar in Costa Rica (10°N, 86°W) and Cariri (7°S, 37°W). *Annales Geophysicae*, 38(6), 1247–1256. <https://doi.org/10.5194/angeo-38-1247-2020>
- Butler, A. H., Seidel, D. J., Hardiman, S. C., Butchart, N., Birner, T., & Match, A. (2015). Defining sudden stratospheric warmings. *Bulletin of the American Meteorological Society*, 96(11), 1913–1928. <https://doi.org/10.1175/BAMS-D-13-00173.1>
- Chang, L., Palo, S., Hagan, M., Richter, J., Garcia, R., Riggins, D., & Fritts, D. (2008). Structure of the migrating diurnal tide in the Whole Atmosphere Community Climate Model (WACCM). *Advances in Space Research*, 41(9), 1398–1407. <https://doi.org/10.1016/j.asr.2007.03.035>
- Chau, J. L., Goncharenko, L. P., Fejer, B. G., & Liu, H.-L. (2012). Equatorial and low latitude ionospheric effects during sudden stratospheric warming events. *Space Science Reviews*, 168(1–4), 385–417. <https://doi.org/10.1007/s11214-011-9797-5>
- Davis, R. N., Du, J., Smith, A. K., Ward, W. E., & Mitchell, N. J. (2013). The diurnal and semidiurnal tides over Ascension Island (8°S, 14°W) and their interaction with the stratospheric quasi-biennial oscillation: Studies with meteor radar, eCMAM and WACCM. *Atmospheric Chemistry and Physics*, 13(18), 9543–9564. <https://doi.org/10.5194/acp-13-9543-2013>
- Dempsey, S. M., Hindley, N. P., Moffat-Griffin, T., Wright, C. J., Smith, A. K., Du, J., & Mitchell, N. J. (2021). Winds and tides of the Antarctic mesosphere and lower thermosphere: One year of meteor-radar observations over Rothera (68°S, 68°W) and comparisons with WACCM and eCMAM. *Journal of Atmospheric and Solar-Terrestrial Physics*, 212, 105510. <https://doi.org/10.1016/j.jastp.2020.105510>
- Eckermann, S. D., & Vincent, R. A. (1994). First observations of intraseasonal oscillations in the equatorial mesosphere and lower thermosphere. *Geophysical Research Letters*, 21(4), 265–268. <https://doi.org/10.1029/93GL02835>
- Eswaraiah, S., Kim, Y. H., Lee, J., Ratnam, M. V., & Rao, S. V. B. (2017). Effect of Southern Hemisphere sudden stratospheric warmings on Antarctica mesospheric tides: First observational study. *Journal of Geophysical Research: Space Physics*, 123, 2127–2140. <https://doi.org/10.1002/2017JA024839>
- Forbes, J. M., Zhang, X., Palo, S., Russell, J., Mertens, C. J., & Mlynarczyk, M. (2008). Tidal variability in the ionospheric dynamo region. *Journal of Geophysical Research*, 113, A02310. <https://doi.org/10.1029/2007JA012737>
- Goncharenko, L., & Zhang, S.-R. (2008). Ionospheric signatures of sudden stratospheric warming: Ion temperature at middle latitude. *Geophysical Research Letters*, 35, L21103. <https://doi.org/10.1029/2008GL035684>
- Goncharenko, L. P., Hsu, V. W., Brum, C. G. M., Zhang, S.-R., & Fentzke, J. T. (2013). Wave signatures in the midlatitude ionosphere during a sudden stratospheric warming of January 2010. *Journal of Geophysical Research: Space Physics*, 118, 472–487. <https://doi.org/10.1029/2012JA018251>
- Griffith, M. J., Dempsey, S. M., Jackson, D. R., Moffat-Griffin, T., & Mitchell, N. J. (2021). Winds and tides of the Extended Unified Model in the mesosphere and lower thermosphere validated with meteor radar observations. *Annales Geophysicae*, 39(3), 487–514. <https://doi.org/10.5194/angeo-39-487-2021>
- Griffith, M. J., & Mitchell, N. J. (2022). Analysis of migrating and non-migrating tides of the Extended Unified Model in the mesosphere and lower thermosphere. *Annales Geophysicae*, 40(3), 327–358. <https://doi.org/10.5194/angeo-40-327-2022>
- Guharay, A., Batista, P. P., Clemesha, B. R., Sarkhel, S., & Buriti, R. A. (2014). Investigation of the intraseasonal oscillations over a Brazilian equatorial station: A case study. *Earth, Planets and Space*, 66(1), 145. <https://doi.org/10.1186/s40623-014-0145-3>

Acknowledgments

This work was supported by the National Natural Science Foundation of China (Grants 42125402, 41974174, 42188101, 41831071, and 42174183), the B-type Strategic Priority Program of CAS (Grant XDB41000000), the Project of Stable Support for Youth Team in Basic Research Field, CAS (Grant YSBR-018), the Open Research Project of Large Research Infrastructures of CAS—Study on the interaction between low/midlatitude atmosphere and ionosphere based on the Chinese Meridian Project, the Fundamental Research Funds for the Central Universities (Grant YD3420002004), the Joint Open Fund of Mengcheng National Geophysical Observatory (MENGO-202209), the Anhui Provincial Natural Science Foundation (Grant 2008085MD113), and the foundation of National Key Laboratory of Electromagnetic Environment (Grant JCKY2020210C614240301). We acknowledge the data resources from the “National Space Science Data Center, National Science & Technology Infrastructure of China (<https://www.nssdc.ac.cn>)”.

- Hagan, M. E., Burrage, M. D., Forbes, J. M., Hackney, J., Randel, W. J., & Zhang, X. (1999). GSWM-98: Results for migrating solar tides. *Journal of Geophysical Research*, *104*(A4), 6813–6827. <https://doi.org/10.1029/1998JA900125>
- He, M., & Chau, J. L. (2019). Mesospheric semidiurnal tides and near-12 h waves through jointly analyzing observations of five specular meteor radars from three longitudinal sectors at boreal midlatitudes. *Atmospheric Chemistry and Physics*, *19*(9), 5993–6006. <https://doi.org/10.5194/acp-19-5993-2019>
- He, M., Chau, J. L., Stober, G., Li, G., Ning, B., & Hoffmann, P. (2018). Relations between semidiurnal tidal variants through diagnosing the zonal wavenumber using a phase differencing technique based on two ground-based detectors. *Journal of Geophysical Research: Atmospheres*, *123*, 4015–4026. <https://doi.org/10.1002/2018JD028400>
- Hocking, W. K., Fuller, B., & Vandeppeer, B. (2001). Real-time determination of meteor-related parameters utilizing modem digital technology. *Journal of Atmospheric and Solar-Terrestrial Physics*, *63*(2–3), 155–169. [https://doi.org/10.1016/S1364-6826\(00\)00138-3](https://doi.org/10.1016/S1364-6826(00)00138-3)
- Hoffmann, P., Singer, W., Keuer, D., Hocking, W. K., Kunze, M., & Murayama, Y. (2007). Latitudinal and longitudinal variability of mesospheric winds and temperatures during stratospheric warming events. *Journal of Atmospheric and Solar-Terrestrial Physics*, *69*(17–18), 2355–2366. <https://doi.org/10.1016/j.jastp.2007.06.010>
- Holdsworth, D. A., Reid, I. M., & Cervera, M. A. (2004). Buckland Park all-sky interferometric meteor radar. *Radio Science*, *39*, RS5009. <https://doi.org/10.1029/2003RS003014>
- Hurrell, J. W., Hack, J. J., Phillips, A. S., Caron, J., & Yin, J. (2006). The dynamical simulation of the Community Atmosphere Model version 3 (CAM3). *Journal of Climate*, *19*(11), 2162–2183. <https://doi.org/10.1175/JCLI3762.1>
- Jiang, G., Xu, J., Shi, J., Yang, G., Wang, X., & Yan, C. (2010). The first observation of the atmospheric tides in the mesosphere and lower thermosphere over Hainan, China. *Chinese Science Bulletin*, *55*(11), 1059–1066. <https://doi.org/10.1007/s11434-010-0084-8>
- Kleinknecht, N. H., Espy, P. J., & Hibbins, R. E. (2014). The climatology of zonal wave numbers 1 and 2 planetary wave structure in the MLT using a chain of Northern Hemisphere Super DARN radars. *Journal of Geophysical Research: Atmospheres*, *119*, 1292–1307. <https://doi.org/10.1002/2013JD019850>
- Lamarque, J.-F., Emmons, L. K., Hess, P. G., Kinnison, D. E., Tilmes, S., Vitt, F., et al. (2012). CAM-Chem: Description and evaluation of interactive atmospheric chemistry in the Community Earth System Model. *Geoscientific Model Development*, *5*(2), 369–411. <https://doi.org/10.5194/gmd-5-369-2012>
- Li, N., Lei, J., Huang, F., Yi, W., Chen, J., Xue, X., et al. (2021). Responses of the ionosphere and neutral winds in the mesosphere and lower thermosphere in the Asian-Australian sector to the 2019 Southern Hemisphere sudden stratospheric warming. *Journal of Geophysical Research: Space Physics*, *126*, 1–15. <https://doi.org/10.1029/2020JA028653>
- Lima, L. M., Alves, E. O., Batista, P. P., Clemesha, B. R., Medeiros, A. F., & Buriti, R. A. (2012). Sudden stratospheric warming effects on the mesospheric tides and 2-day wave dynamics at 7°S. *Journal of Atmospheric and Solar-Terrestrial Physics*, *78*, 99–107. <https://doi.org/10.1016/j.jastp.2011.02.013>
- Liu, G., Janches, D., Lieberman, R. S., Moffat-Griffin, T., Fritts, D. C., & Mitchell, N. J. (2020). Coordinated observations of 8-and 6-hr tides in the mesosphere and lower thermosphere by three meteor radars near 60°S latitude. *Geophysical Research Letters*, *47*, e2019GL086629. <https://doi.org/10.1029/2019GL086629>
- Liu, G., Janches, D., Ma, J., Lieberman, R. S., Stober, G., Moffat-Griffin, T., et al. (2022). Mesosphere and lower thermosphere winds and tidal variations during the 2019 Antarctic Sudden Stratospheric Warming. *Journal of Geophysical Research: Space Physics*, *127*, e2021JA030177. <https://doi.org/10.1029/2021JA030177>
- Lomb, N. R. (1976). Least-squares frequency-analysis of unequally spaced data. *Astrophysics and Space Science*, *39*(2), 447–462. <https://doi.org/10.1007/bf00648343>
- López-González, M. J., Rodríguez, E., García-Comas, M., López-Puertas, M., Olivares, I., Shepherd, M. G., et al. (2017). Semidiurnal tidal activity of the middle atmosphere at mid-latitudes derived from O₂ atmospheric and OH(6–2) airglow SATI observations. *Journal of Atmospheric and Solar-Terrestrial Physics*, *164*, 116–126. <https://doi.org/10.1016/j.jastp.2017.08.014>
- Madden, R. A., & Julian, P. R. (1994). Observations of the 40–50 day tropical oscillation: A review. *Monthly Weather Review*, *122*(5), 814–837. [https://doi.org/10.1175/1520-0493\(1994\)122<0814:OOTDTO>2.0.CO;2](https://doi.org/10.1175/1520-0493(1994)122<0814:OOTDTO>2.0.CO;2)
- Matsuno, T. (1971). A dynamical model of the stratospheric sudden warming. *Journal of the Atmospheric Sciences*, *28*(8), 1479–1494. [https://doi.org/10.1175/1520-0469\(1971\)028<1479:ADMOTS>2.0.CO;2](https://doi.org/10.1175/1520-0469(1971)028<1479:ADMOTS>2.0.CO;2)
- McCormack, J., Hoppel, K., Kuhl, D., de Wit, R., Stober, G., Espy, P., et al. (2017). Comparison of mesospheric winds from a high-altitude meteorological analysis system and meteor radar observations during the boreal winters of 2009–2010 and 2012–2013. *Journal of Atmospheric and Solar-Terrestrial Physics*, *154*, 132–166. <https://doi.org/10.1016/j.jastp.2016.12.007>
- McIntosh, D. L. (2010). *Comparisons of VHF meteor radar observations in the middle atmosphere with multiple independent remote sensing techniques* (Ph.D. dissertation). University of Adelaide. Retrieved from <http://hdl.handle.net/2440/60068>
- McInturf, R. M. (Ed.) (1978). Stratospheric warmings. In *Synoptic, dynamic and general-circulation aspects* (NASA Reference Publ. NASA-RP-1017, p. 174). Retrieved from <http://ntrs.nasa.gov/archive/nasa/casi.ntrs.nasa.gov/19780010687.pdf>
- Murphy, D. J. (2003). Observations of a nonmigrating component of the semidiurnal tide over Antarctica. *Journal of Geophysical Research*, *108*(D8), 4241. <https://doi.org/10.1029/2002JD003077>
- Murphy, D. J., Forbes, J. M., Walterscheid, R. L., Hagan, M. E., Avery, S. K., Aso, T., et al. (2006). A climatology of tides in the Antarctic mesosphere and lower thermosphere. *Journal of Geophysical Research*, *111*, D23104. <https://doi.org/10.1029/2005JD006803>
- Neale, R. B., Richter, J., Park, S., Lauritzen, P., Vavrus, S., Rasch, P., & Zhang, M. (2013). The mean climate of the Community Atmosphere Model (CAM4) in forced SST and fully coupled experiments. *Journal of Climate*, *26*(14), 5150–5168. <https://doi.org/10.1175/JCLI-D-12-00236.1>
- Nischal, N., Oberheide, J., Mlynzcak, M. G., Marsh, D. R., & Gan, Q. (2019). Solar cycle variability of nonmigrating tides in the 5.3 and 15 μ m infrared cooling of the thermosphere (100–150 km) from SABER. *Journal of Geophysical Research: Space Physics*, *124*, 2338–2356. <https://doi.org/10.1029/2018JA026356>
- Oberheide, J., Forbes, J. M., Zhang, X., & Bruinsma, S. L. (2011). Climatology of upward propagating diurnal and semidiurnal tides in the thermosphere. *Journal of Geophysical Research*, *116*, A11306. <https://doi.org/10.1029/2011JA016784>
- Oberheide, J., Wu, Q., Killeen, T. L., Hagan, M. E., & Roble, R. G. (2006). Diurnal nonmigrating tides from TIMED Doppler interferometer wind data: Monthly climatologies and seasonal variations. *Journal of Geophysical Research*, *111*, A10S03. <https://doi.org/10.1029/2005JA011491>
- Ortland, D. A. (2017). Daily estimates of the migrating tide and zonal mean temperature in the mesosphere and lower thermosphere derived from SABER data. *Journal of Geophysical Research: Atmospheres*, *122*, 3754–3785. <https://doi.org/10.1002/2016JD025573>
- Ortland, D. A., & Alexander, M. J. (2006). Gravity wave influence on the global structure of the diurnal tide in the mesosphere and lower thermosphere. *Journal of Geophysical Research*, *111*, A10S10. <https://doi.org/10.1029/2005JA011467>

- Pancheva, D., Mukhtarov, P., Hall, C., Meek, C., Tsutsumi, M., Pedatella, N., et al. (2020). Climatology of the main (24-h and 12-h) tides observed by meteor radars at Svalbard and Tromsø: Comparison with the models CMAM-DAS and WACCM-X. *Journal of Atmospheric and Solar-Terrestrial Physics*, 207, 105339. <https://doi.org/10.1016/j.jastp.2020.105339>
- Paulino, A. R., Batista, P. P., & Clemesha, R. (2011). Lunar tides in the mesosphere and lower thermosphere over Cachoeira Paulista (22.71°S; 45.01°W). *Journal of Atmospheric and Solar-Terrestrial Physics*, 78–79, 31–36. <https://doi.org/10.1016/j.jastp.2011.04.018>
- Pediatella, N. M., & Forbes, J. M. (2010). Evidence for stratosphere sudden warming ionosphere coupling due to vertically propagating tides. *Geophysical Research Letters*, 37, L11104. <https://doi.org/10.1029/2010GL043560>
- Pediatella, N. M., Liu, H. L., & Richmond, A. D. (2012). Atmospheric semidiurnal lunar tide climatology simulated by the Whole Atmosphere Community Climate Model. *Journal of Geophysical Research*, 117, A06327. <https://doi.org/10.1029/2012JA017792>
- Scargle, J. D. (1982). Studies in astronomical time-series analysis. 2. Statistical aspects of spectral-analysis of unevenly spaced data. *The Astrophysical Journal*, 263(2), 835–853. <https://doi.org/10.1086/160554>
- She, C.-Y., Krueger, D. A., Yuan, T., & Oberheide, J. (2016). On the polarization relations of diurnal and semidiurnal tide in the mesopause region. *Journal of Atmospheric and Solar-Terrestrial Physics*, 142, 60–71. <https://doi.org/10.1016/j.jastp.2016.02.024>
- Smith, A. K., Pedatella, N. M., Marsh, D. R., & Matsuo, T. (2017). On the dynamical control of the mesosphere–lower thermosphere by the lower and middle atmosphere. *Journal of the Atmospheric Sciences*, 74(3), 933–947. <https://doi.org/10.1175/jas-d-16-0226.1>
- Sridharan, S., Sathishkumar, S., & Gurubaran, S. (2009). Variabilities of mesospheric tides and equatorial electrojet strength during major stratospheric warming events. *Annales Geophysicae*, 27(11), 4125–4130. <https://doi.org/10.5194/angeo-27-4125-2009>
- Stober, G., Baumgarten, K., McCormack, J. P., Brown, P., & Czarnecki, J. (2020). Comparative study between ground-based observations and NAVGEM-HA analysis data in the mesosphere and lower thermosphere region. *Atmospheric Chemistry and Physics*, 20, 11979–12010. <https://doi.org/10.5194/acp-20-11979-2020>
- Stober, G., Kuchar, A., Pokhotelov, D., Liu, H., Liu, H.-L., Schmidt, H., et al. (2021). Interhemispheric differences of mesosphere–lower thermosphere winds and tides investigated from three whole-atmosphere models and meteor radar observations. *Atmospheric Chemistry and Physics*, 21(18), 13855–13902. <https://doi.org/10.5194/acp-21-13855-2021>
- Watanabe, S., & Miyahara, S. (2009). Quantification of the gravity wave forcing of the migrating diurnal tide in a gravity wave-resolving general circulation model. *Journal of Geophysical Research*, 114, D07110. <https://doi.org/10.1029/2008JD011218>
- Wu, Q., Killeen, T. L., Ortland, D. A., Solomon, S. C., Gablehouse, R. D., Johnson, R. M., et al. (2006). TIMED Doppler interferometer (TIDI) observations of migrating diurnal and semidiurnal tides. *Journal of Atmospheric and Solar-Terrestrial Physics*, 68(3–5), 408–417. <https://doi.org/10.1016/j.jastp.2005.02.031>
- Wu, Q., Ortland, D. A., Killeen, T. L., Roble, R. G., Hagan, M. E., Liu, H.-L., et al. (2008). Global distribution and interannual variations of mesospheric and lower thermospheric neutral wind diurnal tide: 1. Migrating tide. *Journal of Geophysical Research*, 113, A05308. <https://doi.org/10.1029/2007JA012542>
- Wu, Q., Ortland, D. A., Solomon, S. C., Skinner, W. R., & Nijcejewski, R. J. (2011). Global distribution, seasonal, and inter-annual variations of mesospheric semidiurnal tide observed by TIMED TIDI. *Journal of Atmospheric and Solar-Terrestrial Physics*, 73(17), 2482–2502. <https://doi.org/10.1016/j.jastp.2011.08.007>
- Xu, J., Smith, A. K., Jiang, G., Yuan, W., & Gao, H. (2012). Features of the seasonal variation of the semidiurnal, terdiurnal and 6-h components of ozone heating evaluated from Aura/MLS observations. *Annales Geophysicae*, 30(2), 259–281. <https://doi.org/10.5194/angeo-30-259-2012>
- Xu, J., Smith, A. K., Liu, H.-L., Yuan, W., Wu, Q., Jiang, G., et al. (2009). Seasonal and quasi-biennial variations in the migrating diurnal tide observed by Thermosphere, Ionosphere, Mesosphere, Energetics and Dynamics (TIMED). *Journal of Geophysical Research*, 114, D13107. <https://doi.org/10.1029/2008JD011298>
- Yang, C., Smith, A. K., Li, T., & Dou, X. (2018). The effect of the Madden–Julian oscillation on the mesospheric migrating diurnal tide: A study using SD-WACCM. *Geophysical Research Letters*, 45, 5105–5114. <https://doi.org/10.1029/2018GL077956>
- Ye, H., Xue, X., Yu, T., Sun, Y. Y., Yi, W., Long, C., et al. (2021). Ionospheric F-layer scintillation variabilities over the American sector during sudden stratospheric warming events. *Space Weather*, 19, 1–20. <https://doi.org/10.1029/2020SW002703>
- Yi, W., Xue, X., Chen, J., Chen, T., & Li, N. (2019). Quasi-90-day oscillation observed in the MLT region at low latitudes from the Kunming meteor radar and SABER. *Earth and Planetary Physics*, 3(2), 1–11. <https://doi.org/10.26464/epp2019013>
- Younger, P. T., Astin, I., Sandford, D. J., & Mitchell, N. J. (2009). The sporadic radiant and distribution of meteors in the atmosphere as observed by VHF radar at Arctic, Antarctic and equatorial latitudes. *Annales Geophysicae*, 27(7), 2831–2841. <https://doi.org/10.5194/angeo-27-2831-2009>
- Yue, J., Xu, J., Chang, L., Wu, Q., Liu, H.-L., Lu, X., & Russell III, J. (2013). Global structure and seasonal variability of the migrating terdiurnal tide in the mesosphere and lower thermosphere. *Journal of Atmospheric and Solar-Terrestrial Physics*, 105–106, 191–198. <https://doi.org/10.1016/j.jastp.2013.10.010>
- Zhao, L., Chen, J., Ding, Z., Li, N., & Zhao, Z. (2012). First observations of tidal oscillations by an MF radar over Kunming (25.6°N, 103.8°E). *Journal of Atmospheric and Solar-Terrestrial Physics*, 78, 44–52. <https://doi.org/10.1016/j.jastp.2011.04.016>
- Zhou, B. Z., Xue, X. H., Yi, W., Ye, H. L., Zeng, J., Chen, J. S., et al. (2022). A comparison of MLT wind between meteor radar chain data and SD-WACCM results. *Earth and Planetary Physics*, 6(5), 451–464. <https://doi.org/10.26464/epp2022040>